


RESEARCH ARTICLE | APRIL 20 2023

Oblique water entry of an inclined finite plate with gravity effect

Sun Shi Yan (孙士艳) ; Wu G. X. (吴国雄) 



Physics of Fluids 35, 042112 (2023)

<https://doi.org/10.1063/5.0147309>



View
Online



Export
Citation

CrossMark

Articles You May Be Interested In

Effect of entrance portal inclination on the formation of entry compression wave in a high-speed railway tunnel

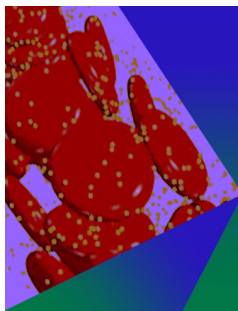
AIP Conference Proceedings (November 2020)

Jet formation and deep seal phenomena associated with inclined oil entry of rotating steel spheres

Physics of Fluids (August 2020)

A numerical study on water entry of cylindrical projectiles

Physics of Fluids (September 2021)



Physics of Fluids

Special Topic: Flow and Forensics

Submit Today!

 AIP
Publishing

 AIP
Publishing

Oblique water entry of an inclined finite plate with gravity effect

Cite as: Phys. Fluids **35**, 042112 (2023); doi: [10.1063/5.0147309](https://doi.org/10.1063/5.0147309)

Submitted: 21 February 2023 · Accepted: 4 April 2023 ·

Published Online: 20 April 2023



View Online



Export Citation



CrossMark

Shi Yan Sun (孙士艳),¹  and G. X. Wu (吴国雄)^{2,a)} 

AFFILIATIONS

¹School of Naval Architecture & Ocean Engineering, Jiangsu University of Science and Technology, Zhenjiang 212003, China

²Department of Mechanical Engineering, University College London, Torrington Place, London WC1E 7JE, United Kingdom

^{a)}Author to whom correspondence should be addressed: g.wu@ucl.ac.uk

ABSTRACT

The hydrodynamic problem of an inclined finite plate entering into water obliquely is investigated through the velocity potential flow theory in the time domain, together with the fully nonlinear boundary conditions on the deforming free surface. A boundary element method is adopted. A stretched coordinate system method is used for the varying computational domain, which starts from a single point at the lower edge of the plate. The whole process of the flow attached on the plate and flow detached from its upper edge is considered, which may involve self-similar flow, transient flow, and steady flow. The gravity effect is also considered. Studies are further conducted for oblique water entry and varying speed entry. Extensive results are provided. Their physical implications and potential applications are discussed.

Published under an exclusive license by AIP Publishing. <https://doi.org/10.1063/5.0147309>

I. INTRODUCTION

Water entry of a finite plate has many engineering applications. One example is a surface piercing propeller (SPP) in naval architecture. The hydrodynamic problem of a propeller is generally three dimensional (3D). However, the section-by-section two-dimensional (2D) theory is commonly used for a blade, such as the well-known lifting line theory.¹ In particular, when the section is sufficiently thin, it is usually simplified as a plate of zero thickness. When a blade emerges from water and then reenters water at high speed, its impact process may be also modeled through section-by-section 2D and each section may be treated as plate.²

When the plate enters water, fluid will depart from the two edges and form a cavity behind the plate. If the gravity effect is ignored at high speed, after sufficiently long time, the flow tends to steady. This is similar to cavity flow in unbounded fluid domain. The analytical solution may be obtained for such a case through conformal mapping method. Typical work includes those by Wu³ and Milne-Thomson.⁴ For the transient problem of water entry at earlier stage, Yim⁵ used a conformal mapping method for a ventilated plate and obtained an analytical solution under the linearized boundary condition on the undisturbed flat free surface. Subsequently, Yim⁶ used this model to further consider difference between water entry and water exit. Wang⁷ also used this model with linearized free surface boundary condition for a plate with small deformation, and conformal mapping method was once again used. The results for complete entry, which means that

the flow on the plate surface has passed its upper edge, were also provided. Wang⁸ further extended the work to the oblique water entry.

For the problem with the nonlinear free surface boundary condition, Chekin⁹ considered the self-similar flow of an inclined semi-infinite plate, using the integral equation method in the complex plane. The free surface in such a case is not known and is a part of the solution. Savineau¹⁰ used the boundary element method (BEM) for a finite curved plate. The cavity shape between the plate edge and the undisturbed free surface was updated during the simulation based on the nonlinear free surface boundary condition. Faltinsen and Semenov¹¹ used the integral hodograph method for the self-similar flow of a semi-infinite plate without gravity effect. The solution was obtained through iteration. It was found that their results for force coefficient and free surface deformation were different from those of Wang^{7,8} based on the linear theory. Vinayan and Kinnas¹² used the BEM together with fully nonlinear boundary conditions to model the water entry of a plate. A small plate was attached to the lower edge of the main plate. The shape of the small plate was based on that of cavity in the unbounded fluid domain.³ The purpose of the small plate was to provide a better initial condition and avoid the numerical difficulty of free surface at the edge of the main plate. The assumption was that the effect of the small plate will diminish at later stage. They have undertaken simulations in the context of SPP. Simulation of water entry of a plate related to SPP has also been performed through a more general computational fluid dynamics (CFD) method. Viscous flow theory is usually used, based on

the Navier–Stokes equations. Typical work includes those by Ghadimi and Javanmardi¹³ for a falling foil with flow detaching from the leading edge and forming different types of trapped bubbles, and Javanmardi and Ghadimi² considered a similar case, but with the elastic effect of the leading edge. Mesa *et al.*¹⁴ solved problem for the water entry of an inclined elastic plate. Moradi *et al.*¹⁵ adopted a hybrid method combining the Wagner theory and the Fluent software. Khabakhpasheva and Korobkin¹⁶ considered the water entry of an elastic plate into shallow water. When the deadrise angle between the plate and free surface becomes zero, the problem will turn into a horizontal plate impacting on water surface. Typical work includes those by Iafrazi and Korobkin,^{17,18} Krechetnikov,¹⁹ and Sun and Wu.²⁰

In the above work, it is common that either the model is linear, or the plate is semi-infinite, or the gravity effect is ignored, or the entry speed is constant. Thus, it is the purpose of the present work to consider the water entry problem of a finite plate at varying speed with gravity effect. Fully nonlinear boundary conditions on the deforming free surface shape will be used. The boundary element method will be adopted, which has been successfully used by the authors for related problems.^{20,21} In Sec. II, we shall first outline the mathematical model of an inclined finite plate entering into water. The governing equation and boundary conditions are introduced based on the velocity potential theory. The stretched coordinate system used for early stage is outlined. In Sec. III, the boundary element method, the method for calculation of pressure, and the treatment of flow separation from the edges are provided. In Sec. IV, a convergence study is conducted and comparison is made, followed by extensive simulations for oblique entry of a finite plate at varying speed with gravity and detailed discussions of the results.

II. MATHEMATICAL MODEL

We consider the problem of an inclined plate of length c impacting a horizontal free surface (Fig. 1). A Cartesian coordinate system $O - x_0y_0$ is defined. x_0 is along the undisturbed free surface, y_0 points vertically upwards, and the origin is fixed at the point where the tip of the plate touches the free surface initially. The plate has an inclined angle γ with x_0 axis and a velocity $\mathbf{U} = ui - vj$, where u and v are the velocity components in the x_0 and y_0 directions, respectively, and negative sign before v means that it is positive when the plate goes into the water. $\alpha_0 = \text{atan}(v/u)$ is the angle between \mathbf{U} and x_0 axis. The velocity \mathbf{U} of the plate is prescribed, which can be either constant or varying.

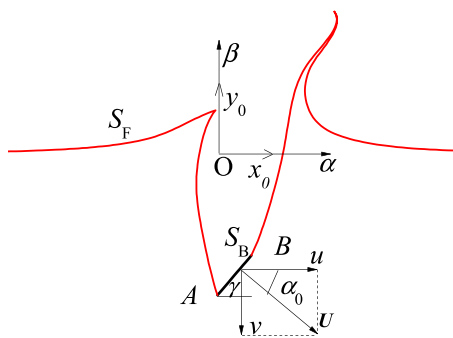


FIG. 1. Sketch of problem.

The fluid is assumed to be ideal and incompressible, and the flow is irrotational. The velocity potential theory can then be used. The governing equation for the potential ϕ can be written as

$$\nabla^2 \phi = 0 \tag{1}$$

in the fluid domain. On the plate surface S_b , the impermeable boundary condition gives

$$\phi_n = un_{x_0} - vn_{y_0}, \tag{2}$$

where $\mathbf{n} = (n_{x_0}, n_{y_0})$ is the normal of the body surface, pointing away from the fluid domain. On the free surface S_f , the Lagrangian form of the kinematic and dynamic conditions can be, respectively, written as

$$\frac{dx_0}{dt} = \phi_{x_0}, \quad \frac{dy_0}{dt} = \phi_{y_0}, \tag{3}$$

$$\frac{d\phi}{dt} = \frac{1}{2} (\phi_{x_0}^2 + \phi_{y_0}^2) - gy_0, \tag{4}$$

where g is the acceleration due to gravity, and the temporal derivative d/dt is taken by following a fluid particle. In the Eulerian form, the kinematic and dynamic conditions can be written as

$$\frac{\partial y_0}{\partial t} = \phi_{y_0} - \frac{\partial y_0}{\partial x_0} \phi_{x_0}, \tag{5}$$

$$\frac{\partial \phi}{\partial t} = -\frac{1}{2} (\phi_{x_0}^2 + \phi_{y_0}^2) - gy_0, \tag{6}$$

where the temporal derivative is taken when x_0 and y_0 are fixed. Away from the plate, the fluid is assumed to be undisturbed by the plate motion.

A particular feature of this kind of problem is that at the initial stage, there is only a small part of the body in contact with water, or the wetted surface is small. This part will increase as the plate moves into the water. This means that initially the disturbed region of the fluid is small, while within this region, the flow varies rapidly. To capture this variation, the size of a typical element used in a numerical method must be much smaller than that of the wetted surface. Later on, the disturbed region will increase. To continue to use small elements would mean that a large number of them would be needed. Therefore, the element size should increase as the plate moves into water. To achieve this more effectively, we may use the stretched coordinate system method.²² Let s be the vertical distance of the plate traveled into the water. We define

$$\alpha = x_0/s, \quad \beta = y_0/s, \quad \varphi = \phi/(sv). \tag{7}$$

This means that both the coordinates and the potential have been amplified by s . In such a way, the size of the disturbed domain remains more or less the same at the earlier stage when s is small and at the later stage when s is large. The element size and the element number can also remain more or less the same. When s is comparable to the dimension of the plate, for example, its vertical height $c \sin \gamma$, the computation may be conducted directly in the $O - x_0y_0$ system.

Then, Eq. (1) will retain its form for φ , while Eqs. (2)–(4) become

$$\varphi_n = \varepsilon n_x - n_\beta \quad \text{on } S_b, \tag{8}$$

$$\frac{ds\alpha}{dt} = v\varphi_\alpha, \quad \frac{ds\beta}{dt} = v\varphi_\beta \quad \text{on } S_f, \tag{9}$$

$$\frac{dsv\varphi}{v^2 dt} = \frac{1}{2} (\varphi_\alpha^2 + \varphi_\beta^2) - \frac{gs\beta}{v^2} \quad \text{on } S_f, \quad (10)$$

where $\varepsilon = u/v = 1/\tan\alpha_0$. It should be noted that the normal derivative in Eq. (8) is taken in the (α, β) system and

$$\frac{\partial}{\partial n} \Big|_{(x_0, y_0)} = \frac{1}{s} \frac{\partial}{\partial n} \Big|_{(\alpha, \beta)} \quad (11)$$

has been used. Similarly, Eqs. (5) and (6) may be written as

$$\frac{\partial s\beta}{v\partial t} = \varphi_\beta - \beta_\alpha \varphi_\alpha, \quad (12)$$

$$\frac{\partial s v \varphi}{v^2 \partial t} = -\frac{1}{2} (\varphi_\alpha^2 + \varphi_\beta^2) - \frac{gs\beta}{v^2}. \quad (13)$$

Using $ds/dt = v$ and noticing $d/dt = vd/ds$, these two equations may be also written as

$$\beta = \varphi_\beta - \eta_\alpha \varphi_\alpha + \alpha \varphi_\alpha, \quad (14)$$

$$\varphi + \frac{s\varphi\dot{v}}{v^2} + s \frac{\partial \varphi}{\partial s} = -\frac{1}{2} (\varphi_\alpha^2 + \varphi_\beta^2) + \alpha \varphi_\alpha + \beta \varphi_\beta - \frac{gs\beta}{v^2}, \quad (15)$$

where over dot means the derivative with respect to time. If the gravity effect is neglected, the flow on the plate has not passed its top tip, or point B , and $\frac{dv}{v}$ is constant, then the similarity solution with $\frac{\partial \varphi}{\partial s} = 0$ would exist.¹⁸ In particular for a semi-infinite plate with $\dot{v} = 0$, these conditions are clearly met. This is in fact the problem considered by Faltinsen and Semenov¹¹ for a semi-infinite plate.

III. NUMERICAL PROCEDURE

We adopt the boundary element method to solve the present problem. The Laplace equation in the fluid domain is first converted into an integral equation over the whole boundary S through Green's identity,

$$A(p)\varphi(p) = \int_S \left(\ln r_{pq} \frac{\partial \varphi(q)}{\partial n_q} - \varphi(q) \frac{\partial \ln r_{pq}}{\partial n_q} \right) ds, \quad (16)$$

where $A(p)$ is the solid angle at the point p on the boundary, and r_{pq} is the distance from the field point p to the source point q . The integration in (16) is performed with respect to q . The boundary S contains the plate surface S_b , free surface S_f , and a control surface S_c away for the body, where the disturbance to the fluid by the plate is assumed to be insignificant. To solve (16) numerically, S is first divided into many small elements. As in Sun and Wu,²⁰ Sun *et al.*,²¹ and Wu *et al.*,²² here the straight-line element will be used and variables are assumed to vary linearly within each element. From (8), the normal derivative of the potential on the plate surface S_b is known. On the free surface, the potential is assumed to be zero initially. Subsequently, it is obtained through time stepping based on (10) together with the free surface shape being updated through (9). Therefore, the potential on S_f is

known. On the control surface S_c , φ_n is set as zero since the disturbance is assumed to have diminished at the far field. These conditions are imposed on the nodes of the elements, and as a result, a set of linear equations is obtained. Through the solution, the unknowns are found at each time step.

To start the simulation, an initial condition has to be prescribed. Physically, as only a very small region of the fluid domain is disturbed, this is not expected to have lasting effect on the flow at the later stage. However, numerically a proper treatment of the initial condition is important for the simulation. Here, in the stretched system, the initial configuration at $s = s_0$ is given in Fig. 2. On the right-hand side, the free surface is assumed to be undisturbed. On the left, the local free surface near the tip of the plate is assumed to be perpendicular to the plate and then joins the undisturbed main free surface, and $\varphi = 0$ is assumed on the free surface.

When the boundary integral equation is solved for the potential at each given time step, the pressure p can then be obtained through the Bernoulli equation. In the dimensionless form, the pressure coefficient can be written as

$$C_p = \frac{p}{\rho v^2/2} = -\left(\frac{2\phi_t}{v^2} + |\nabla\varphi|^2 + \frac{2gs\beta}{v^2} \right), \quad (17)$$

where the temporal derivative of ϕ is taken for fixed x_0 and y_0 . We note that in the equation, even when the velocity potential φ or ϕ has been obtained at each time step numerically, ϕ_t is still not explicitly known if the solution is not self-similar. Here, we employ the approach developed by Wu and Taylor.^{23,24} ϕ_t satisfies the Laplace equation. Its free surface boundary condition can be obtained from pressure $p = 0$. The body surface boundary condition for ϕ_t can be written as²⁵

$$\begin{aligned} \frac{\partial \phi_t}{\partial n} &= \dot{u}n_x - \dot{v}n_y - u \frac{\partial \phi_x}{\partial n} + v \frac{\partial \phi_y}{\partial n} \\ &= \dot{u}n_x - \dot{v}n_y - uv \frac{\partial \varphi_\alpha}{\partial n} + v^2 \frac{\partial \varphi_\beta}{\partial n}. \end{aligned} \quad (18)$$

We may, then, define

$$\phi_t = v^2 \chi + s\dot{u}\chi_1 - s\dot{v}\chi_2 - \varepsilon v^2 \varphi_\alpha + v^2 \varphi_\beta. \quad (19)$$

The auxiliary functions χ , χ_1 , and χ_2 all satisfy the Laplace equation in the fluid domain. We may impose

$$\frac{\partial \chi}{\partial n} = 0, \quad \frac{\partial \chi_1}{\partial n} = n_x, \quad \frac{\partial \chi_2}{\partial n} = n_\beta \quad (20)$$

on the body surface in the (α, β) system. Then, noticing Eq. (11), Eq. (18) is satisfied in the (x_0, y_0) system. To satisfy pressure $p = 0$ on the free surface, we impose

$$\chi = -\left(\frac{1}{2} |\nabla\varphi|^2 + \frac{gs\beta}{v^2} \right) + \varepsilon \varphi_\alpha - \varphi_\beta, \quad \chi_1 = 0, \quad \chi_2 = 0. \quad (21)$$

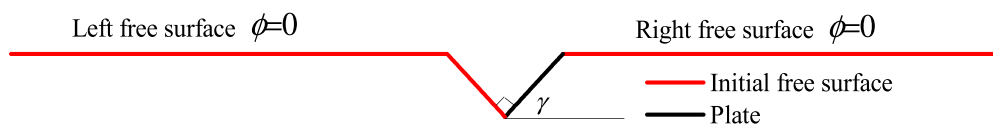


FIG. 2. Initial configuration and condition.

At the far field, where the disturbance diminishes, the boundary condition can be written as

$$\frac{\partial \chi}{\partial n} = 0, \quad \frac{\partial \chi_1}{\partial n} = 0, \quad \frac{\partial \chi_2}{\partial n} = 0. \quad (22)$$

The auxiliary functions can, then, be solved in the stretched coordinate system in the same way used for φ . Once they are found, the temporal derivative of ϕ can be obtained from Eq. (19), which can, then, be used in Eq. (17) for the pressure.

As illustrated in Fig. 1, the flow detaches from the lower and eventually upper edges of a finite plate or points A and B, respectively. These two points are also on the free surface, and fluid velocity there is assumed to be continuous. Because of the impermeable condition on the body surface, the velocity at two points is, therefore, tangential to the plate. The potentials at A and B are updated at each time step by following these two points. The time derivative defined in this way can be written as

$$\frac{\delta}{\delta t} = \frac{\partial \phi}{\partial t} + u\phi_{x_0} - v\phi_{y_0}, \quad (23)$$

where δ means the variation of ϕ fixed on the plate edge. The partial derivative ϕ_t in this equation can be obtained from the Bernoulli equation with $p = 0$. Thus, we have

$$\frac{\delta s v \varphi}{\nu^2 \delta t} = -\frac{1}{2} (\varphi_x^2 + \varphi_y^2) - \frac{g s \beta}{\nu^2} + \varepsilon \varphi_x - \varphi_\beta \quad \text{on } S_f. \quad (24)$$

IV. NUMERICAL RESULTS AND DISCUSSIONS

A. Convergence study and comparison

In order to test the numerical stability and accuracy of the method in the paper, the case of a plate with infinite length entering into water vertically is first considered. The gravity effect is neglected or g is set as zero. The flow in such a case is self-similar and has been considered by Falinsen and Semenov.¹¹ In such a case, the problem is independent of s , and the solution can be given in the dimensionless system (α, β) . s or t is merely a parameter used for stepping, and its dimension is not essential. The simulation starts at $s = s_0$. It should be noted that no matter how small s_0 is, the vertical distance between point A and the still water surface is always unit in the stretched

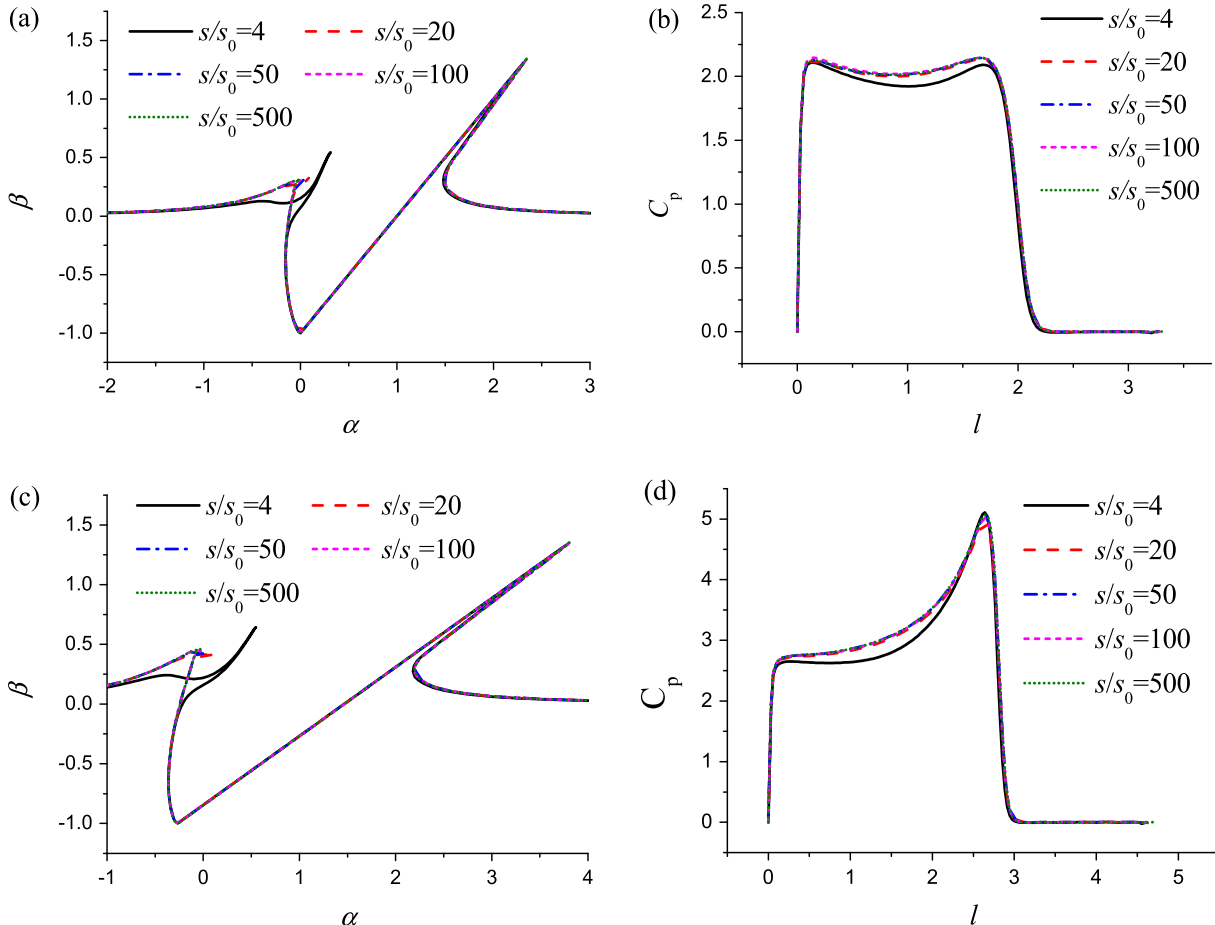


FIG. 3. Effect of the initial condition and configuration: (a) the free surface profile ($\gamma = 45^\circ$ and $\alpha_0 = 90^\circ$), (b) the pressure distribution on the plate ($\gamma = 45^\circ$ and $\alpha_0 = 90^\circ$), (c) the free surface profile ($\gamma = 30^\circ$ and $\alpha_0 = 105^\circ$), and (d) the pressure distribution on the plate ($\gamma = 30^\circ$ and $\alpha_0 = 105^\circ$) ($l_m = 0.03$, $\delta = 1.02$, $d s_0 = 5 \times 10^{-9}$, $\tau = 1.002$, and $k_1 = 20$).

system. The length and the depth of the rectangular computational domain are, respectively, set as 60 and 30 in the stretched system. Unequal elements are distributed along the fluid boundary. The body surface and part of the free surface between the jet tip and the plate edge are distributed with elements with equal size, denoted as l_m , and the size of the element along the free surface away from the jet tip and plate increases gradually at a fixed ratio δ and is not allowed to be larger than 0.5. We set the time increment as $ds = \min [\tau^{n-1} ds_0, l_m / (k_1 |\nabla \phi|_{\max})]$, where $\tau > 1$ and $k_1 > 1$ are fixed constants, n means the n th time step, and $|\nabla \phi|_{\max}$ is the largest velocity of fluid particle on the free surface. The first step ds_0 at $n = 1$ is the smallest, and the step, then, increases at a fixed ratio τ . The step is not allowed to be larger than $l_m / (k_1 |\nabla \phi|_{\max})$, or a fluid particle is not allowed to move more than a fraction of the element length.

Figure 3 gives some snapshots of the free surface and pressure coefficient from the mesh of typical element size being $l_m = 0.03$ and $\delta = 1.02$ at $\gamma = 45^\circ$ and $\alpha_0 = 90^\circ$ and $\gamma = 30^\circ$ and $\alpha_0 = 105^\circ$, respectively. The latter corresponds to oblique entry. The attack angle, which is

the angle between U and the plate AB , or $180^\circ - \gamma - \alpha_0$, for both cases is 45° . The calculation starts with an initial value $s_0 = 10^{-5}$ and the configuration in Fig. 2, and $ds_0 = 5 \times 10^{-9}$, $k_1 = 20$, and $\tau = 1.002$. l in the figure is the length along the plate measured from the point A in

Fig. 1 in the stretched system, or $l = \sqrt{(\alpha - \alpha_A)^2 + (\beta - \beta_A)^2}$. As the initial condition is not self-similar, we notice that in Fig. 3 that there is an obvious transition period when $s/s_0 < 20$. Beyond that the transient behavior becomes far less evident and almost vanishes completely after $s/s_0 \approx 50$. In fact, the results from $s/s_0 = 50$ and $s/s_0 = 500$ are virtually indistinguishable, which shows that the self-similarity of the flow has been achieved. This means that at a given s_0 the results at $s > 50s_0$ are not very much affected by the initial condition at s_0 , or to ensure the result at a given s is not too much affected by the initial condition, we can always set $s_0 < s/50$. It is also interesting to see at the same attack angle, the results are different at different γ and α_0 , or the self-similar solution depends on them separately.

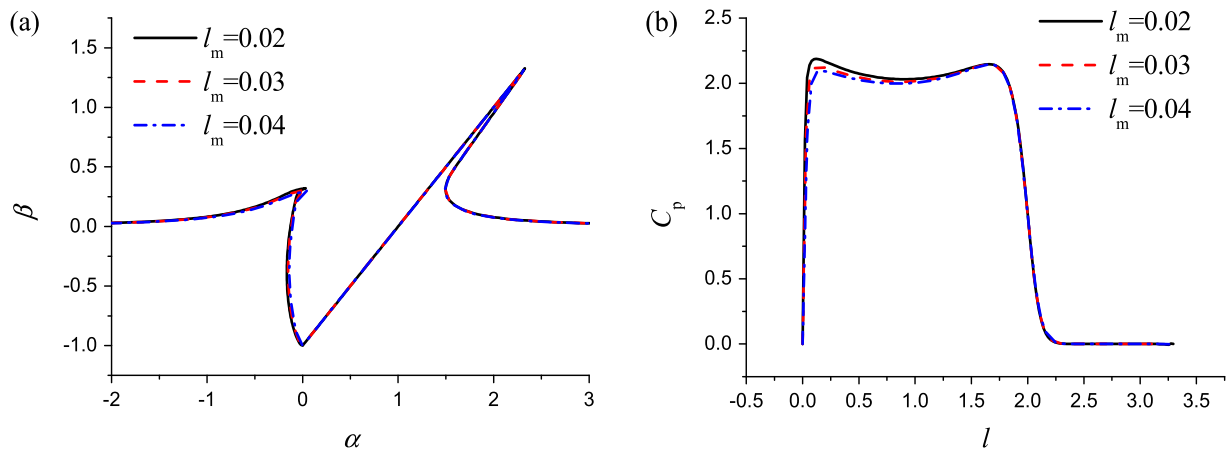


FIG. 4. Mesh convergence study ($\gamma = 45^\circ$ and $\alpha_0 = 90^\circ$): (a) the free surface profile and (b) the pressure distribution on the plate ($s/s_0 = 50$, $\delta = 1.02$, $ds_0 = 2 \times 10^{-9}$, $\tau = 1.002$, and $k_1 = 20$).

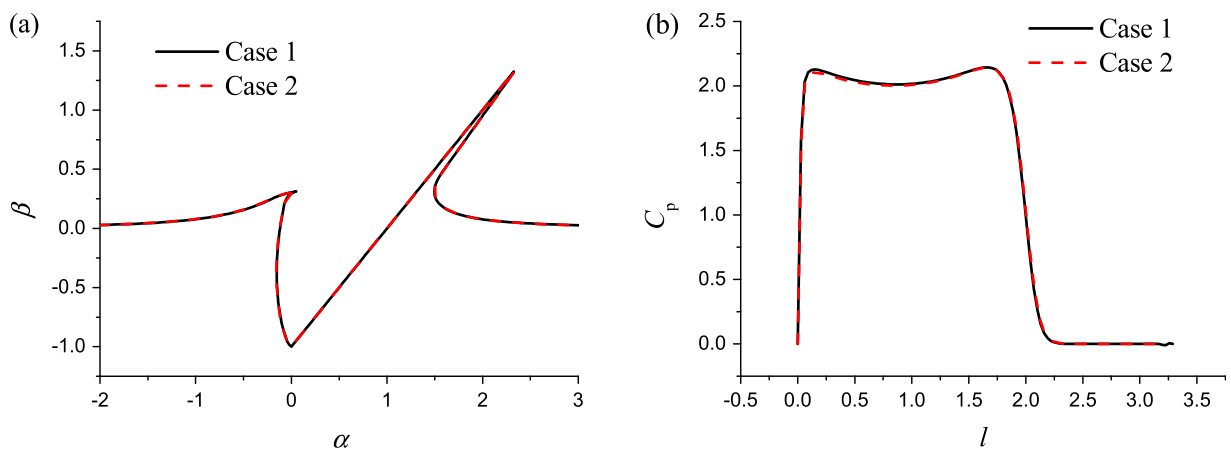


FIG. 5. Time step convergence study ($\gamma = 45^\circ$ and $\alpha_0 = 90^\circ$): (a) the free surface profile and (b) the pressure distribution on the plate ($s/s_0 = 50$, $l_m = 0.03$ and $\delta = 1.02$).

Downloaded from http://pubs.aip.org/aip/pof/article-pdf/doi/10.1063/5.0147309/16898013042112_1_5.0147309.pdf

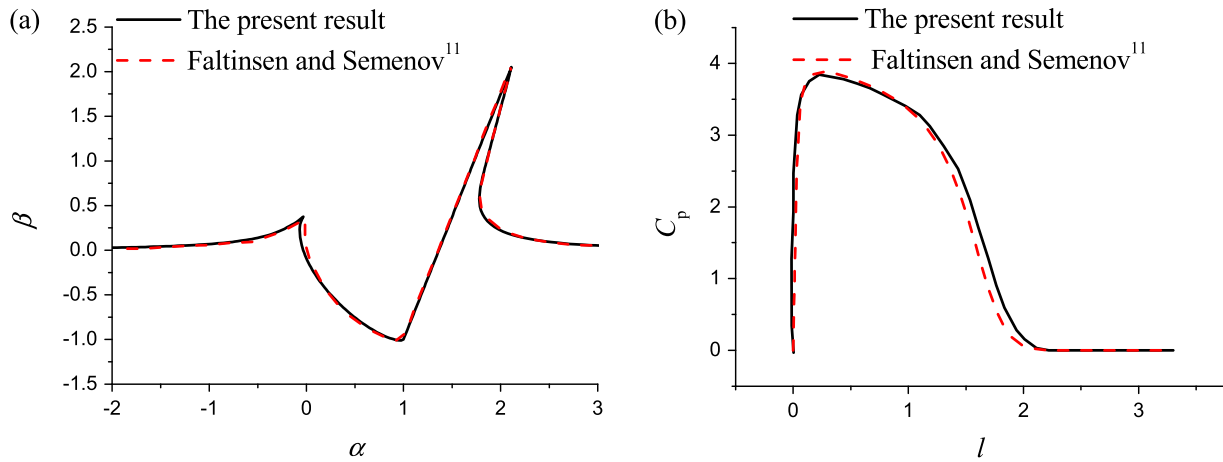


FIG. 6. Comparison with the results by Faltinsen and Semenov¹¹ ($\gamma = 70^\circ$ and $\alpha_0 = 45^\circ$): (a) free surface and (b) pressure.

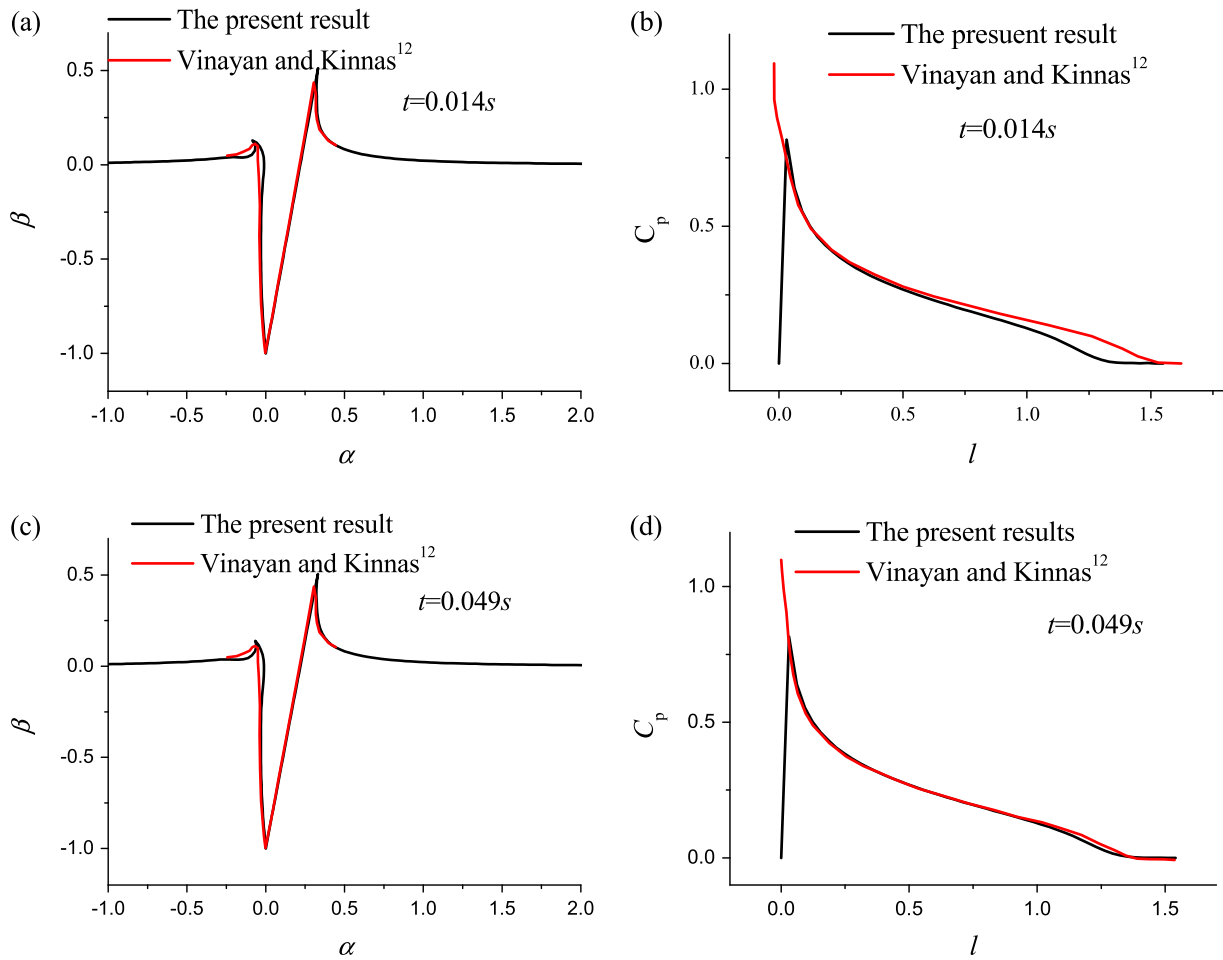


FIG. 7. Comparison with the result by Vinayan and Kinnaas¹² ($\gamma = 77.614^\circ$, $\alpha_0 = 90^\circ$, and $v = 2.45$ m/s): (a) free surface at $t = 0.014$ s, (b) pressure at $t = 0.014$ s, (c) free surface at $t = 0.049$ s, and (d) pressure at $t = 0.049$ s.

Downloaded from http://pubs.aip.org/aip/pof/article-pdf/doi/10.1063/5.0147309/1689801.3042112_1.5.0147309.pdf

To investigate the mesh convergence, we set the element length l_m near the plate edge as 0.04, 0.03, and 0.02, respectively, for the case of $\gamma = 45^\circ$ and $\alpha_0 = 90^\circ$, and the element size increases ratio $\delta = 1.02$. The free surface profile and the pressure distribution from these three different meshes are shown in Fig. 4. A good agreement can be seen in the figure, and this verifies that these results are mesh independent. Unless it is specified, in the following simulations, the minimal element length $l_m = 0.03$ and the element size increase ratio $\delta = 1.02$ are chosen.

Figure 5 gives comparison between the results at $s/s_0 = 50$ for $\gamma = 45^\circ$, $\alpha_0 = 90^\circ$, with two different time steps. In case 1, $ds_0 = 5 \times 10^{-9}$, $k_1 = 20$, $\tau = 1.002$, and in case 2, $ds_0 = 2.5 \times 10^{-9}$, $k_1 = 40$, $\tau = 1.001$. It can be seen that the two curves for free surfaces are graphically indistinguishable, and those for pressure coefficients also coincide well. This shows the time step convergence of the numerical procedure. Unless it is specified, $ds_0 = 5 \times 10^{-9}$, $k_1 = 20$, and $\tau = 1.002$ are used in the following simulations.

In order to verify the accuracy of the results, we make a comparison first with the self-similar solution by Faltinsen and Semenov.¹¹ The deadrise angle γ is set as 70° , and the direction of U is set as $\alpha_0 = 45^\circ$, which is an oblique entry. Good agreement can be seen

in Fig. 6. Vinayan and Kinnas¹² also considered the problem of impact by an inclined plate, using the boundary element method. To initiate the simulation, they added a small plate at the tip of the main plate. The shape of the small plate followed that of the surface of the supercavity, derived from the analytical solution by Wu³ for a plate in the unbounded fluid domain. The length of the small plate is chosen to be a small fraction of the length of the inclined plate. Initially, this is in fact a solution for a wedge if the curvature of the small plate is negligible. After the flow has passed the edge of the small plate and the simulation continues, the effect of the small plate is assumed to diminish gradually and the solution tends to that of the inclined plate. The purpose of this small plate is in fact to avoid the numerical difficulties due to the singularity around the tip of the inclined plate, which could affect the free surface development. The inclusion of the small plate moves the intersection of the free surface and the body to the tip of the small plate. The angle between the symmetry line of the wedge and the vertical direction is 10° , and the inner angle of the wedge is 4.772° , which corresponds to a deadrise angle γ of 77.614° in the present work. The entry velocity v is set as 2.45 m/s with $\alpha_0 = 90^\circ$, as in their work. Figure 7 provides a comparison between the present results and those from Vinayan and Kinnas¹² just before the flow departs from

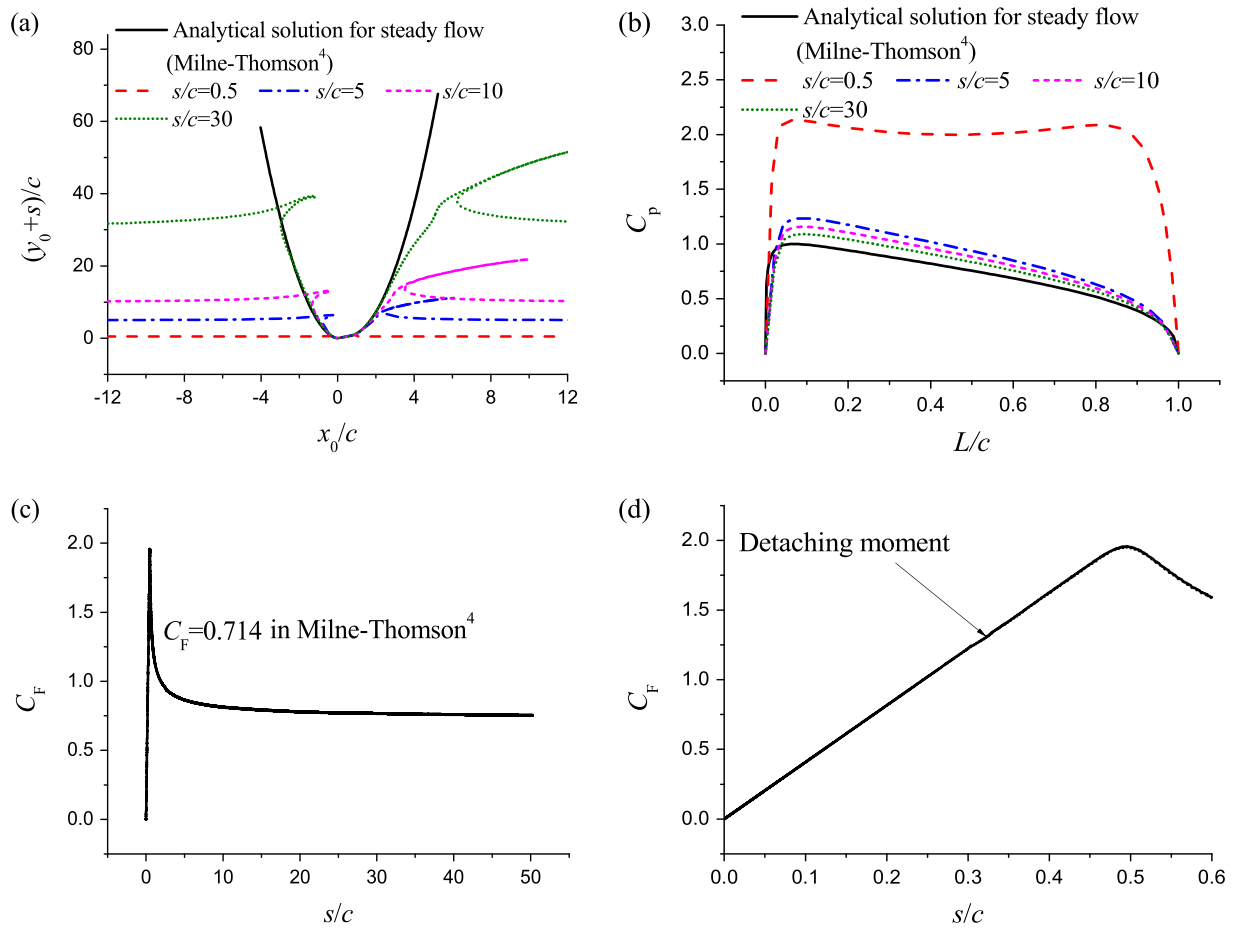


FIG. 8. Water entry of a finite plate without gravity effect ($\gamma = 45^\circ$ and $\alpha_0 = 90^\circ$): (a) free surface, (b) pressure, (c) force coefficient, and (d) early stage of (c).

Downloaded from http://pubs.aip.org/aip/pof/article-pdf/doi/10.1063/5.0147309/16899013042112_1.5.0147309.pdf

point *B*. Good agreements can be seen from the figure, except for the local pressure at the lower plate edge, or point *A*. Since this is the intersection point with the free surface, the pressure there should be zero, as in the present solution. The result from Vinayan and Kinnas¹² is not zero, as a small plate is used on the left and the edge is not the intersection point with the free surface. In fact, with a small plate, local flow at the tip is similar to that of a wedge entering water. The pressure at the tip can be singular, and numerical result can change sharply.²¹

B. Finite plate

1. Constant speed without gravity effect

We undertake a detailed study for a plate with finite length *c* and entering water with vertical speed *v*. ρ , *c*, and *v* are used for nondimensionalization in this section. Two cases are provided. For case 1, γ is set as 45° and $\alpha_0 = 90^\circ$, for case 2, $\gamma = 30^\circ$, $\alpha_0 = 105^\circ$, as in Fig. 3, and the attack angle in these two cases is 45°. The half width and depth of the computational domain in the present case is set as around four times the length between the point *A* and the highest point of jet

tip, and gravity effect is ignored. Figures 8 and 9 provide the free surfaces and pressure coefficients after the flow has departed from the upper edge of the plate and the time history of force coefficient $C_F = F/(\frac{1}{2}\rho v^2 c)$, in which *F* is the total force in the direction perpendicular to the plate. In the following figures, *L* is to denote the distance to point *A* in the physical system $O - x_0 y_0$.

The simulation is done in the stretched system with varying *s* until $s = c \sin \gamma$. After that, the simulation is done in the physical system. At the earlier stage during the entry, the flow is self-similar before the flow detaches from the upper tip, or point *B*, and a thin jet is fully attached to the body surface, for which the free surface shapes and pressures are already seen in Fig. 3. Within this, period C_p does not change with time and therefore, $C_F = \frac{1}{c} \int_{S_b} C_p ds = \frac{s}{c} \int_{S_b} C_p dl$ increases linearly with *s*, as can be seen when $s/c \leq 0.32$ in Fig. 8 and $s/c \leq 0.22$ in Fig. 9(d). After that, the attached thin jet starts leaving the plate from point *B*. As the pressure in the thin jet is almost zero, departure of the thin jet from point *B* does not affect the linear behavior of C_F with *s* initially. This will continue until $s/c \approx 0.5$ in Fig. 8(d) and $s/c \approx 0.4$ in Fig. 9(d), at which moment the jet root has detached from the body, and C_F has reached the peak. Figures 8(a), 8(b), 9(a),

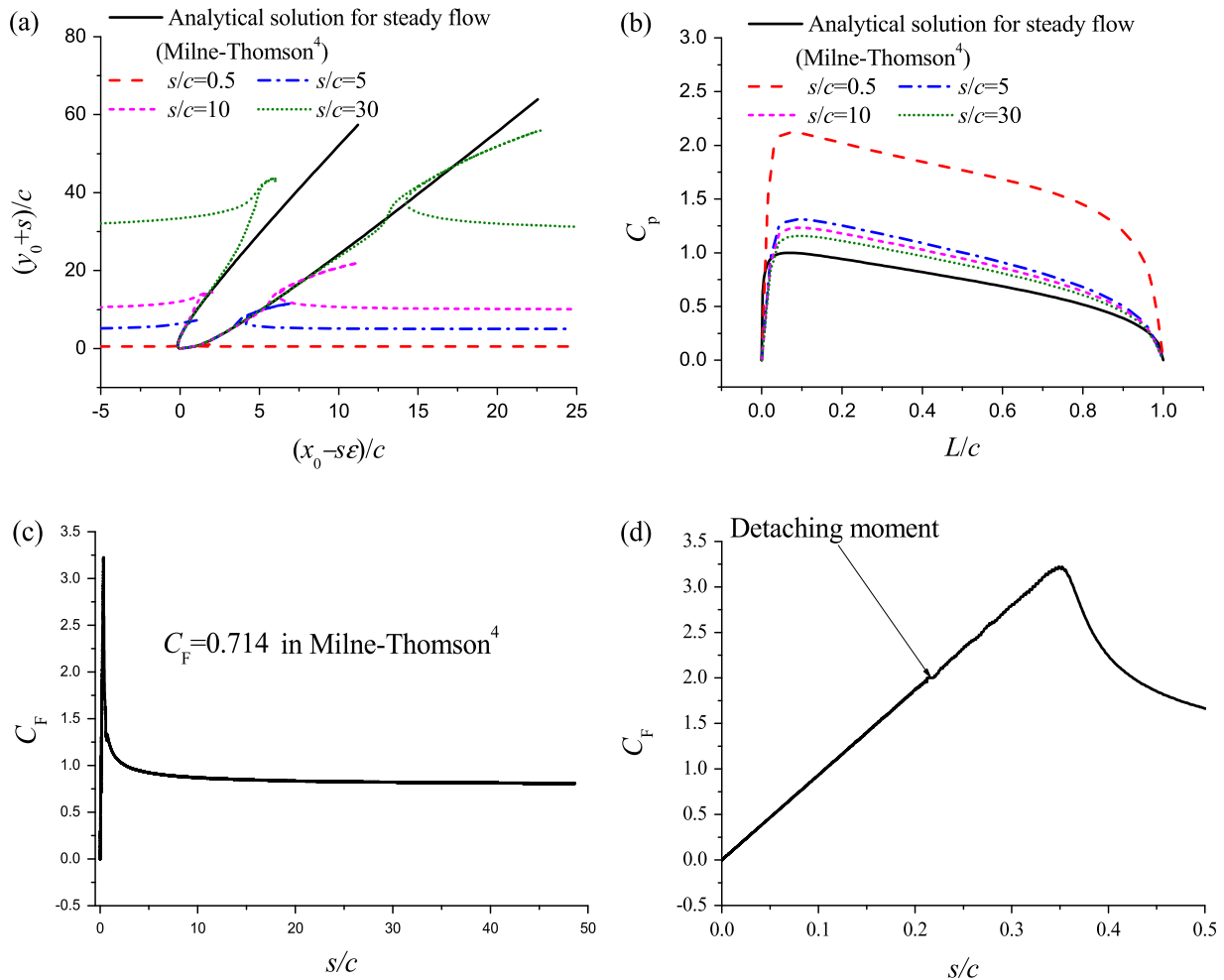


FIG. 9. Water entry of a finite plate without gravity effect ($\gamma = 30^\circ$ and $\alpha_0 = 105^\circ$): (a) free surface, (b) pressure, (c) force coefficient, and (d) early stage of (c).

Downloaded from http://pubs.aip.org/aip/pof/article-pdf/doi/10.1063/5.0147309/1689801.3042112_1.5.0147309.pdf

and 9(b) provide snapshots of the free surfaces and pressures for $s/c > 0.5$. It can be seen that the pressure drops quickly with s at first and the decrease gradually becomes milder. Thus, C_F in Figs. 8 and 9(c) also decrease rapidly first and then mildly. As the plate further travels down, the free surface shape near the plate gradually becomes stable and tends to that from the steady solution of a cavity flow in the unbounded domain obtained from Milne-Thomson⁴ (also see the Appendix). Correspondingly, as s increases, the pressure in Figs. 8 and 9(b) becomes closer to that of Milne-Thomson.⁴ A relatively small difference at $s/c = 30$ is still visible, due to the effect of unsteady free surface motion away from the plate. It is expected that as the plate further goes down or s/c tends to infinity, this difference would disappear.

2. Constant speed with gravity effect

We now consider the gravity effect through the Froude number defined as $F_n = v/\sqrt{gc}$. The gravity effect depends on both the Froude number and time. At a small Froude number, the gravity effect may become important at very early stage, while at a large Froude number, it becomes important only at late stage. We undertake simulations at Froude numbers $F_n = 0.714, 1.428, \text{ and } 2.143$ and provide results at

different s . Let $\gamma = 45^\circ$ and $\alpha_0 = 90^\circ$. In Figs. 10(a) and 10(b), when $s/c = 2.5 \times 10^{-3}$, which is before flow detachment from B , the free surfaces and pressures for different Froude numbers are close to each other, and this is because when t or s is small, the gravity effect is weak. However, in Fig. 10(c) when $s/c = 1$, the gravity effect becomes significant, and it can clearly be seen that the jet will be pulled down by the gravity. When the Froude number is smaller, the gravity effect is more prominent, the jet will be lower, and Fig. 10(c) reflects this fact. Special attention should be paid to the free surface on the left-hand side, where the jet tip bends down and forms an overturning jet. It can be seen that the jet corresponding to $F_n = 0.714$ almost hits the plate at $s/c = 1$. When it happens, a closed air bubble can be formed. The problem beyond that can be solved by using the method in Sun *et al.*,²⁶ but it is beyond the scope of the current work. For the pressure in Fig. 10(d), due to the gravity effect, when F_n is smaller the pressure is larger.

For a propeller blade at a given radius, v corresponds to the blade vertical speed and u corresponds to the water advance speed. Here, we will investigate the variation of pressures at different u . We set $\varepsilon = u/v = 0, 0.1, 0.2$, respectively, which corresponds to $\alpha_0 = 90^\circ, 84.33^\circ, 78.73^\circ$, respectively. The Froude number is 0.714. The deadrise

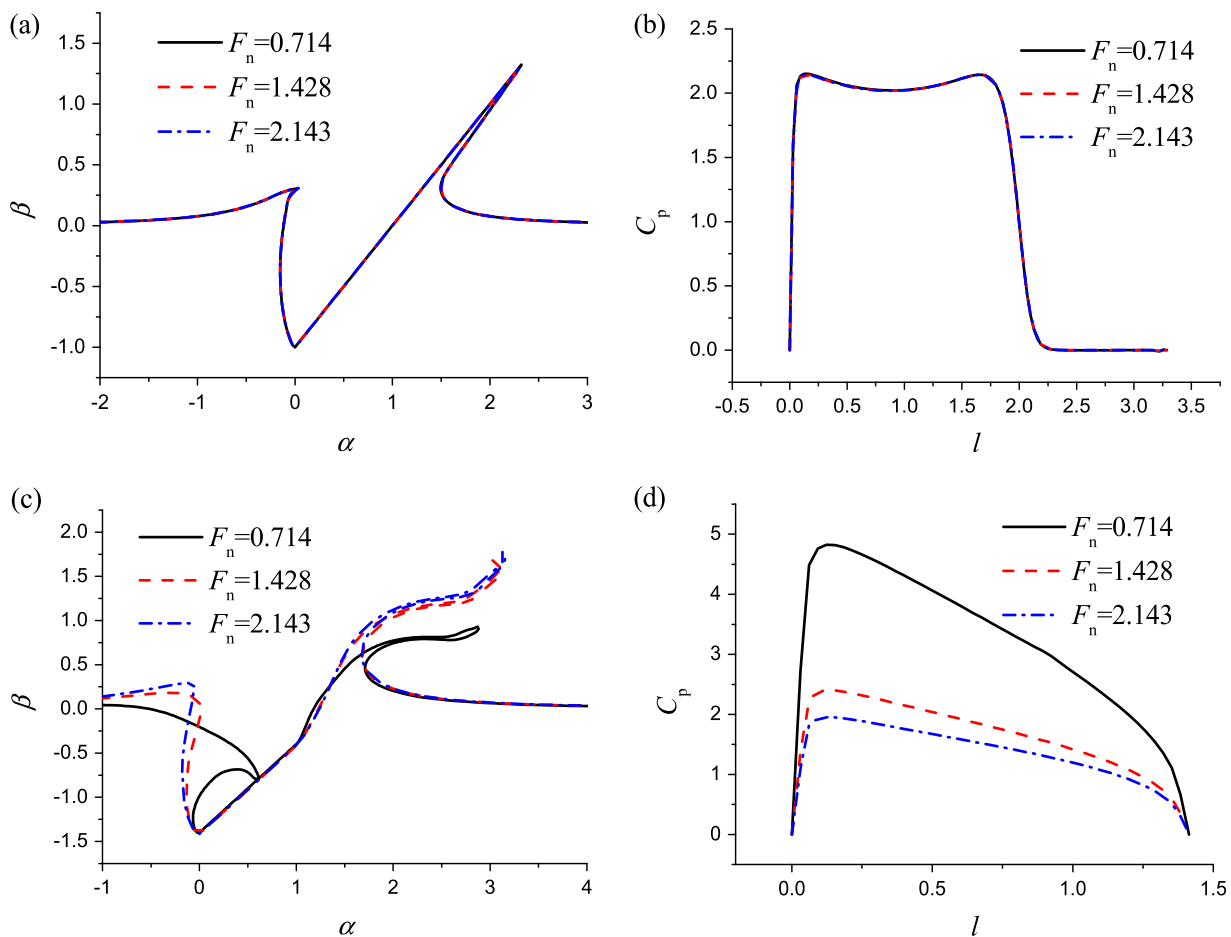


FIG. 10. Water entry of an inclined plate with finite length with gravity effect ($\gamma = 45^\circ$ and $\alpha_0 = 90^\circ$): (a) free surface at $s/c = 2.5 \times 10^{-3}$, (b) pressure at $s/c = 2.5 \times 10^{-3}$, (c) free surface at $s/c = 1$, and (d) pressure at $s/c = 1$.

Downloaded from http://pubs.aip.org/aip/pof/article-pdf/doi/10.1063/5.0147309/16898013042112_1_5.0147309.pdf

angle $\gamma = 45^\circ$. Here, pressure coefficient C_u is defined through the magnitude of \mathbf{U} or $C_u = C_p \sin^2 \alpha_0$. At the earlier stage $s/c = 2.5 \times 10^{-3}$, the gravity effect is smaller (Fig. 11). The solution is closer to the self-similar one and the pressure is very much affected by

u . At $s/c = 0.5$, the difference between results at different u is much smaller. It is interesting to see at $s/c = 1.0$, the difference is further reduced. In fact, when the gravity is ignored, the pressure at large s/c will tend to that in Eq. (A5), where $\alpha_1 = \pi - \alpha_0 - \gamma$. The curves from

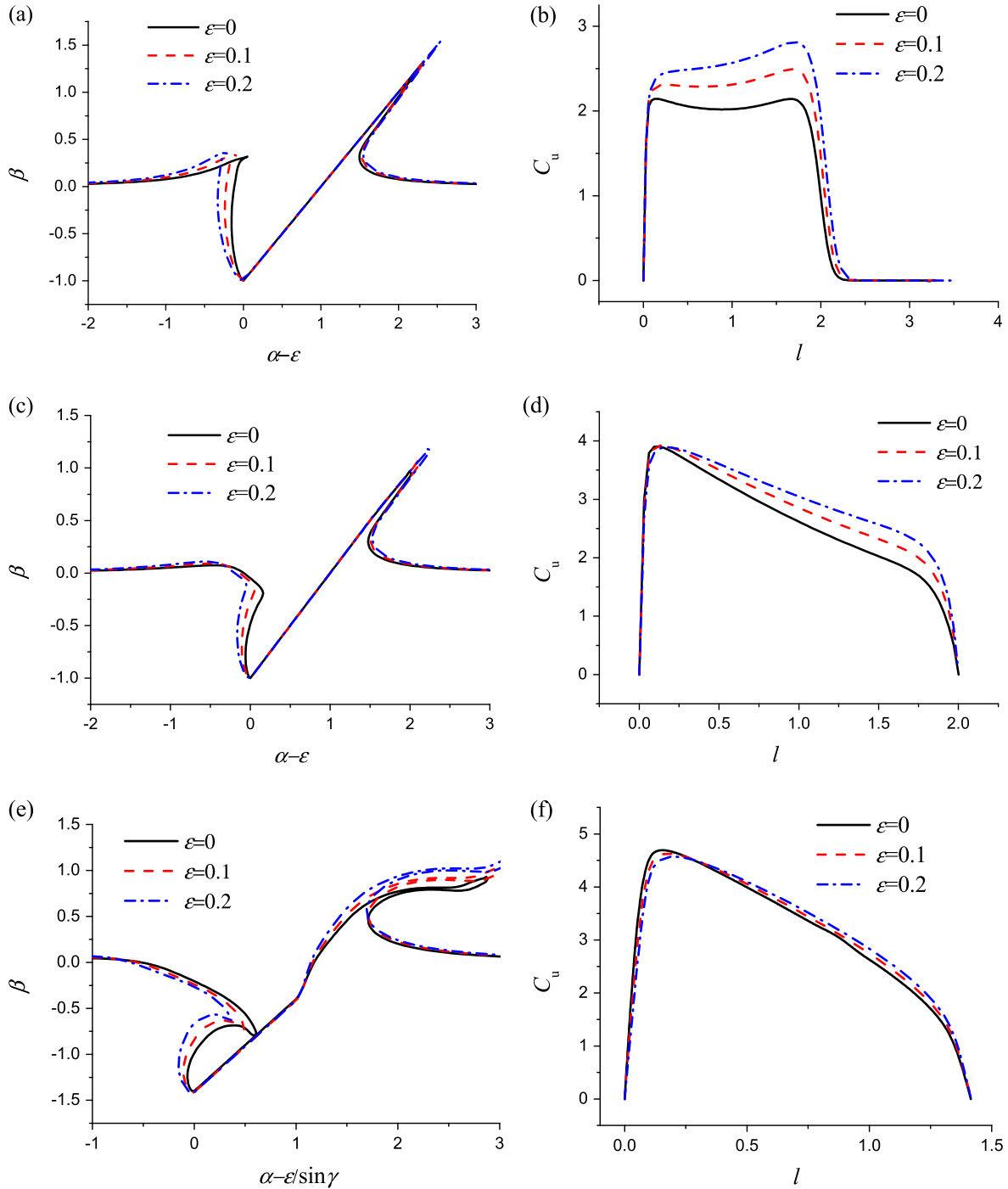


FIG. 11. Water entry of a plate with finite length with gravity ($F_n = 0.714$, $\gamma = 45^\circ$): (a) free surface ($s/c = 2.5 \times 10^{-3}$), (b) pressure ($s/c = 2.5 \times 10^{-3}$), (c) free surface ($s/c = 0.5$), (d) pressure ($s/c = 0.5$), (e) free surface ($s/c = 1$), and (f) pressure ($s/c = 1$).

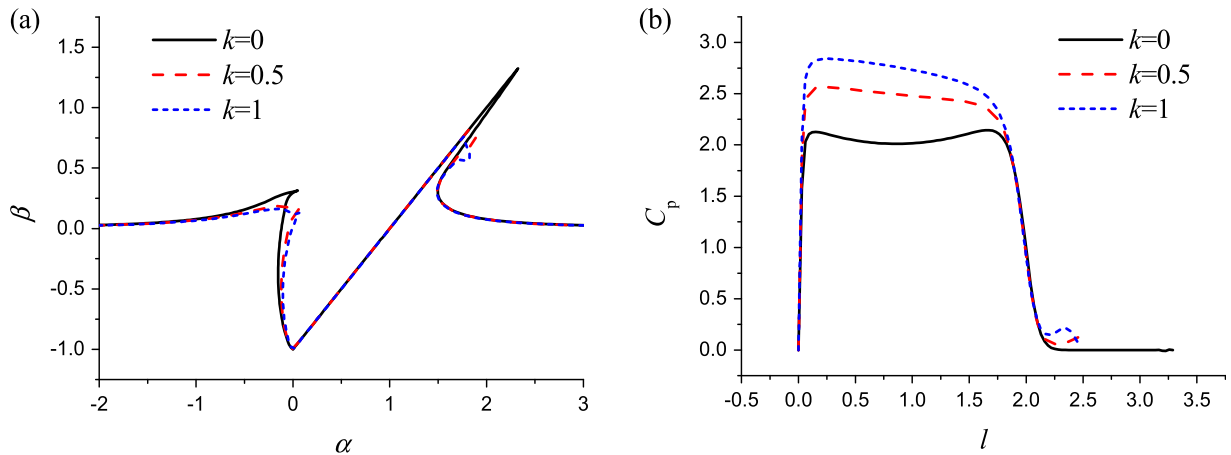


FIG. 12. Water entry of a semi-infinite plate without gravity ($\gamma = 45^\circ$ and $\alpha_0 = 90^\circ$): (a) free surface and (b) pressure.

this equation at $\alpha_0 = 90^\circ, 84.33^\circ, 78.73^\circ$ can be found to be quite close to each other.

3. Varying speed

If we set $v = At^k$ for the case with varying speed, then we have $\frac{dv}{v^2} = \frac{k}{k+1}$, which is constant. In such a case, the solution is self-similar if the gravity is ignored as discussed after Eqs. (14) and (15). The flow becomes fully transient after separation from point B occurs. We set $\gamma = 45^\circ$, $\alpha_0 = 90^\circ$, and choose $k = 0, 0.5, 1$ to see the effect of k on the solution. When $k = 0$, the plate travels down with constant velocity, which has been considered previously. For the case of $k = 0.5$, the plate has varying acceleration, which is infinite at $t = 0$, and then decreases. For $k = 1$, the plate has constant acceleration. Figure 12 gives the self-similar solution. The inertial force is related to $\frac{dv}{v^2} \chi_2 = \frac{k}{k+1} \chi_2$. χ_2 mainly depends on deadrise angle γ , as can be seen from its boundary conditions in Eqs. (20)–(22). The coefficient $\frac{k}{k+1} = 0, \frac{1}{3}, \frac{1}{2}$ when $k = 0, 0.5, 1$, respectively. This indicates that the inertial force increases with k , which is part of the reason that the pressure coefficient in Fig. 12(b) is larger at larger k . The free surface in

Fig. 12(a), on the other hand, is lower at larger k . When $k = 0$, there is a thin jet attached to the plate. When $k \neq 0$, the jet region becomes thicker and a hump is formed near the intersection of the body surface and the free surface. Correspondingly, there is a local hump in the pressure coefficient in Fig. 12(b), which is similar to what has been observed on a wedge.²¹

The above case is vertical entry corresponding to $\alpha_0 = 90^\circ$. We further consider the oblique entry with $\alpha_0 = 80^\circ$ and 70° , respectively. The free surface and the pressure coefficient C_u are provided in Fig. 13. k is set as 0.5, and $\frac{dv}{v^2} = \frac{dv}{v^2} = \frac{dk}{k+1}$. The deadrise angle remains as $\gamma = 45^\circ$, and therefore, the attack angle is $45^\circ, 55^\circ, 65^\circ$, respectively. This means that the attack angle between U and the plate increases as α_0 decreases, or flow direction moves toward the normal direction. As a result, the pressure is larger at smaller α_0 or larger attack angle, as shown in Fig. 13(b).

V. CONCLUSIONS

The problem of an inclined plate entering into calm water is investigated through the velocity potential flow theory together with the boundary element method and the stretched coordinate system

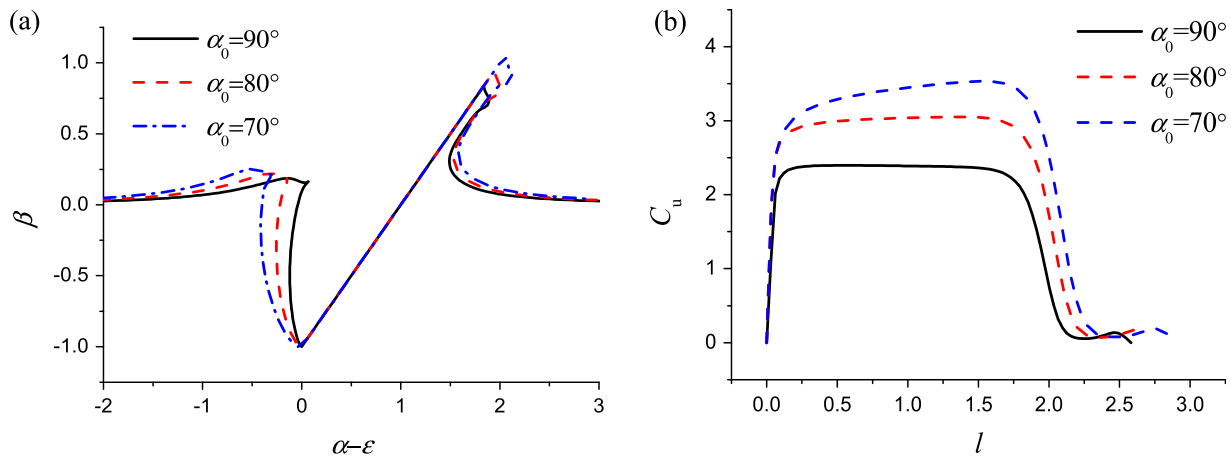


FIG. 13. Water entry of a plate with infinite length without gravity with $\gamma = 45^\circ$: (a) free surface and (b) pressure.

method. Extensive results are provided, for cases of a semi-infinite plate and finite plate, vertical entry and oblique entry, constant speed and varying speed, and without and with gravity effect. From these, the following conclusions can be drawn.

- (1) When simulation starts an entry distance $s = s_0$, the effect of the initial condition will diminish around $s > 50s_0$. For a semi-infinite plate at a constant speed or before the flow passes the upper edge of a finite plate, the numerical solution tends to be self-similar.
- (2) For a finite plate, the flow can be self-similar before it passes the upper edge. After the detachment, the flow is transient. As the entry continues, the flow will eventually become steady if the gravity is ignored and tends to the cavity flow in the unbounded fluid domain.
- (3) When the flow is self-similar, the force coefficient C_F increases linearly with the entry distance s . It remains approximately the case even when jet on the plate has passed its upper tip and continues until the jet root is leaving the upper edge. After that, C_F drops rapidly first and then mildly and tends to that of the steady flow in the unbounded fluid domain when the gravity effect is neglected.
- (4) The gravity effect is weak at the initial stage. Its effect will increase as water entry continues, and becomes significant at earlier stage if the Froude number is lower. The gravity effect can pull down the jet, which may hit the plate or the main free surface.
- (5) For oblique entry, the self-similarity will depend on the flow direction and the deadrise angle of the plate. For steady flow of a finite plate, it does not depend on them separately and depends on only the angle between the flow direction and the plate.

ACKNOWLEDGMENTS

This work was supported by the National Natural Science Foundation of China (Grant No. 52271276).

AUTHOR DECLARATIONS

Conflict of Interest

The authors have no conflicts to disclose.

Author Contributions

Shi Yan Sun: Investigation (equal); Writing – original draft (equal).
Guoxiong Wu: Supervision (equal); Writing – review & editing (equal).

DATA AVAILABILITY

The data that support the findings of this study are available within the article.

APPENDIX: FREE SURFACE SHAPE, PRESSURE, AND FORCE FOR STEADY FLOW DERIVED FROM THE SOLUTION OF MILNE-THOMSON⁴

Figure 14 shows a uniform stream with velocity U from infinity passes a stationary plate AB , as in Milne-Thomson.⁴ Here, $\alpha_1 = \pi - \alpha_0 - \gamma$, and $k = \frac{\sin \alpha_1}{2} + \frac{2}{\pi}$. From the solution in Milne-Thomson,⁴ we may obtain the following results:

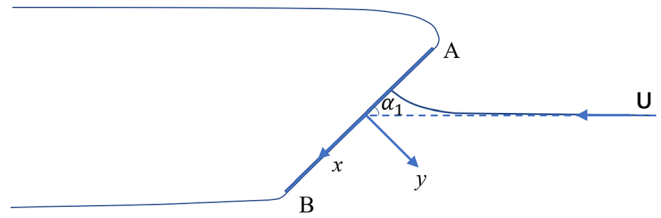


FIG. 14. A uniform flow from infinity impinges on a plate AB (Milne-Thomson⁴).

- (1) Free surface initiated from B , $\zeta \in (1, \infty)$,

$$(x - x_B)/c = \frac{1}{k\pi} \left[\frac{1}{2} \cos \alpha_1 (\zeta^2 - 1) + \zeta - 1 \right], \tag{A1}$$

$$(y - y_B)/c = \frac{\sin \alpha_1}{2\pi k} \left[-\zeta \sqrt{\zeta^2 - 1} + \ln \left(\zeta + \sqrt{\zeta^2 - 1} \right) \right]. \tag{A2}$$

- (2) Free surface initiated from A , $\zeta \in (-1, -\infty)$,

$$(x - x_A)/c = \frac{1}{k\pi} \left[\frac{1}{2} \cos \alpha_1 (\zeta^2 - 1) + \zeta + 1 \right], \tag{A3}$$

$$(y - y_A)/c = \frac{\sin \alpha_1}{2\pi k} \left[\zeta \sqrt{\zeta^2 - 1} + \ln \left(-\zeta + \sqrt{\zeta^2 - 1} \right) \right]. \tag{A4}$$

- (3) The pressure coefficient on the plate, $\zeta \in (-1, 1)$,

$$C_p = 1 - \left\{ \frac{(\zeta + \cos \alpha_1)}{1 + \cos \alpha_1 \zeta + \sin \alpha_1 \sqrt{1 - \zeta^2}} \right\}^2. \tag{A5}$$

- (4) The force coefficient

$$C_F = \frac{2\pi \sin \alpha_1}{4 + \pi \sin \alpha_1}. \tag{A6}$$

REFERENCES

- ¹J. N. Newman, *Marine Hydrodynamics* (The MIT Press Cambridge, Massachusetts, 2017).
- ²N. Javanmardi and P. Ghadimi, "Hydroelastic analysis of surface piercing hydrofoil during initial water entry phase," *Sci. Iran., Trans. B* **26**, 295–310 (2019).
- ³Y. T. Wu, "A free streamline theory for two-dimensional fully cavitated hydrofoils," *J. Math. Phys.* **35**, 236–265 (1956).
- ⁴L. M. Milne-Thomson, *Theoretical Hydrodynamics* (London Macmillan & CO LTD., London, 1962).
- ⁵B. Yim, "An application of linearized theory to water entry and water exit problem. Part 2. With ventilation," *Research and Development Report 3171* (Naval Ship Research and Development Center, Washington, D.C., USA, 1970).
- ⁶B. Yim, "Linear theory on water entry and exit problems of a ventilating thin wedge," *J. Ship Res.* **18**, 1–11 (1974).
- ⁷D. P. Wang, "Water entry and exit of a fully ventilated foil," *J. Ship Res.* **21**, 44–68 (1977).
- ⁸D. P. Wang, "Oblique water entry and exit of a fully ventilated foil," *J. Ship Res.* **23**, 43–54 (1979).
- ⁹B. S. Chekin, "The entry of a wedge into an incompressible fluid," *J. Appl. Math. Mech.* **53**, 300–307 (1989).
- ¹⁰M. Savineau, "A time marching boundary element method for the prediction of the flow around surface piercing hydrofoils," M.S. thesis (Massachusetts Institute of Technology, 1996).
- ¹¹O. M. Faltinsen and Y. Semenov, "Nonlinear problem of flat-plate entry into an incompressible liquid," *J. Fluid Mech.* **611**, 151–173 (2008).

Downloaded from http://pubs.aip.org/aip/article-pdf/doi/10.1063/5.0147309/1689801/3042112_1_5.0147309.pdf

- ¹²V. Vinayan and S. Kinnas, "A numerical nonlinear analysis of two-dimensional ventilating entry of surface-piercing hydrofoils with effects of gravity," *J. Fluid Mech.* **658**, 383–408 (2010).
- ¹³P. Ghadimi and N. Javanmardi, "Analysis of ventilation regimes of the oblique wedge-shaped surface piercing hydrofoil during initial water entry process," *Pol. Marit. Res.* **25**, 33–43 (2018).
- ¹⁴J. D. Mesa, K. J. Maki, and M. T. Graham, "Numerical analysis of the impact of an inclined plate with water at high horizontal velocity," *J. Fluids Struct.* **114**, 103684 (2022).
- ¹⁵H. Moradi, A. R. Ranji, H. Haddadpour, and H. Moghadas, "A hybrid model for simulation of fluid–structure interaction in water entry problems," *Phys. Fluids* **33**, 017102 (2021).
- ¹⁶T. I. Khabakhpasheva and A. A. Korobkin, "Oblique elastic plate impact on thin liquid layer," *Phys. Fluids* **32**, 062101 (2020).
- ¹⁷A. Iafrati and A. A. Korobkin, "Initial stage of flat plate impact onto liquid free surface," *Phys. Fluids* **16**, 2214 (2004).
- ¹⁸A. Iafrati and A. A. Korobkin, "Hydrodynamic loads during early stage of flat plate impact onto water surface," *Phys. Fluids* **20**, 082104 (2008).
- ¹⁹R. Krechetnikov, "Origin of ejecta in the water impact problem," *Phys. Fluids* **26**, 052105 (2014).
- ²⁰S. Y. Sun and G. X. Wu, "Local flow at plate edge during water entry," *Phys. Fluids* **32**, 072103 (2020).
- ²¹S. Y. Sun, S. L. Sun, and G. X. Wu, "Oblique water entry of a wedge into waves with gravity effect," *J. Fluids Struct.* **52**, 49–64 (2015).
- ²²G. X. Wu, H. Sun, and Y. S. He, "Numerical simulation and experimental study of water entry of a wedge in free fall motion," *J. Fluids Struct.* **19**, 277–289 (2004).
- ²³G. X. Wu and R. E. Taylor, "Transient motion of a floating body in steep waves," in *11th Workshop on Water Waves and Floating Bodies*, Hamburg, Germany, 1996.
- ²⁴G. X. Wu and R. E. Taylor, "The coupled finite element and boundary element analysis of nonlinear interactions between waves and bodies," *Ocean Eng.* **30**, 387–400 (2003).
- ²⁵G. X. Wu, "Hydrodynamic force on a rigid body during impact with liquid," *J. Fluids Struct.* **12**, 549–559 (1998).
- ²⁶S. Y. Sun, G. X. Wu, and G. Xu, "Breaking wave impact on a floating body with air bubble effect," *J. Fluids Struct.* **82**, 16–34 (2018).